

RSC Advances

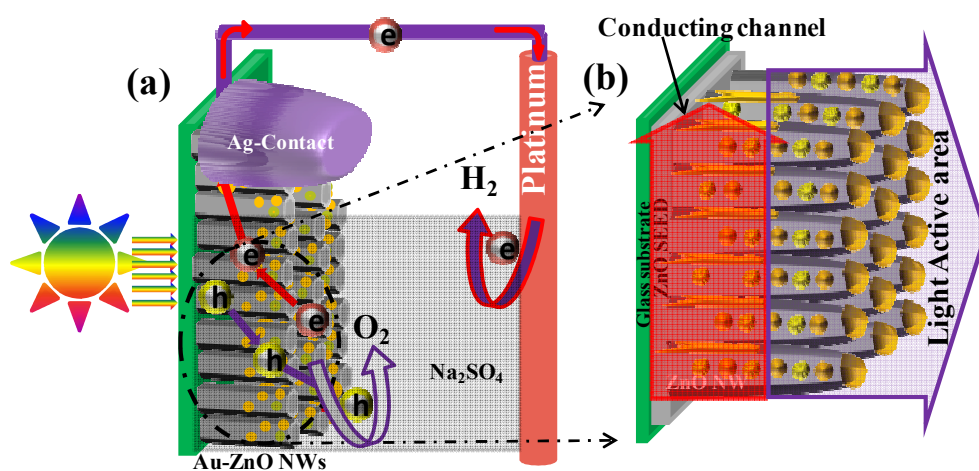


This is an *Accepted Manuscript*, which has been through the Royal Society of Chemistry peer review process and has been accepted for publication.

Accepted Manuscripts are published online shortly after acceptance, before technical editing, formatting and proof reading. Using this free service, authors can make their results available to the community, in citable form, before we publish the edited article. This *Accepted Manuscript* will be replaced by the edited, formatted and paginated article as soon as this is available.

You can find more information about *Accepted Manuscripts* in the [Information for Authors](#).

Please note that technical editing may introduce minor changes to the text and/or graphics, which may alter content. The journal's standard [Terms & Conditions](#) and the [Ethical guidelines](#) still apply. In no event shall the Royal Society of Chemistry be held responsible for any errors or omissions in this *Accepted Manuscript* or any consequences arising from the use of any information it contains.



ITO/FTO free AuNPs functionalized ZnO NWs photoanode in dual role such as photo active centers for catalytic activity and an efficient transport medium for photo-generated charge carriers.

Cite this: DOI: 10.1039/c0xx00000x

www.rsc.org/xxxxxx

ARTICLE TYPE

Defect controlled water splitting characteristics of gold nanoparticles functionalized ZnO nanowire films

Ajay Kushwaha and M. Aslam*

Received (in XXX, XXX) XthXXXXXXXXXX 20XX, Accepted Xth XXXXXXXXXXXXX 20XX

DOI: 10.1039/b000000x

Functionalization of ZnO nanowire by size controlled gold nanoparticles is demonstrated through sputtering of gold layer followed by annealing at different temperature. Rationally designed sputtered Au nanoparticles - ZnO nanowire (AuNP-ZnO) exhibit high photocatalytic activity for water splitting. The tailored structure shows an enhanced photocurrent of 300 $\mu\text{A}/\text{cm}^2$ under visible light illumination. To further add, the efficiency of 0.13% at a low bias of 0.45 V vs Ag-AgCl, indicates an efficient charge separation and collection without a conducting ITO/FTO base. The AuNPs tune the visible light absorption and utilize the SPR of Au nanoparticle to boost the hot electron injection from the Au nanoparticles to ZnO conduction band. Moreover, AuNPs also assists in suppression of surface defects of ZnO NWs (or hole traps) significantly and enhance the water splitting performance of the material under visible light.

1. Introduction

High electron mobility and ease of fabrication makes ZnO nanowires a suitable material for photoelectrochemical (PEC) water splitting in comparison to other metal oxides such as TiO_2 and WO_3 .^{1,2-3} Poor visible light absorption, rapid recombination of photo-generated charge carriers (high concentration of surface traps) and photo-corrosion of ZnO in electrolyte solution are some of the major obstacles towards practical realization of ZnO nanowire films as photoanode.^{4,5-10} Various surface functionalization strategies such as metal/semiconductor NPs decoration, dye sensitization and core-shell structure formation have been explored by different research groups to overcome above mentioned challenges.^{6,11-16} For example, metal nanoparticle coated oxide photoanodes (TiO_2 , Fe_2O_3 and ZnO) have shown reduction in trap states due to surface passivation, and an improvement in visible light absorption thus proving their worth as photoanode.¹⁶⁻²⁰ Functionalization of TiO_2 films with gold, silver and platinum nanoparticles have rendered a significant improvement (60 times) in photocatalytic activity.^{19,21,22} In a similar manner, gold nanoparticle decorated ZnO or Fe_2O_3 nanoplatelets have also shown higher absorption of visible light leading to an improved photocatalytic behavior.¹⁶⁻¹⁸ In most of these studies, metal nanoparticles are considered as an antenna for the light absorption and semiconductor nanostructure platform acts as a reaction center for photocatalytic activity.¹⁶ Similarly, it is also proposed that gold acts as an electron trapping center for photo-generated charges

and escalates separation rate of electron-hole pairs in photocatalytic activity.^{20,18} In addition, formation of Schottky junction between silver nanoparticles and ZnO microrod is believed to be a cause of an effective separation of photo-generated charges.²³ In a similar manner, AuNPs coating also forms a Schottky barrier at ZnO-Au interface and prevents a reverse transfer of holes from the electrolyte leading to a reduction in recombination of photo-generated charge carriers.²⁴ Furthermore, the size of the metal nanoparticles is also a decisive parameter to control the range and intensity of visible light absorption and hence optimizes the intensity of localized electric field at the metal-semiconductor interface.^{25,26} In a nutshell, transfer of excitation energy of metal nanoparticles to semiconductor creates electro-hole pairs at photo anode surface and therefore directly contributes to PEC performance.

Despite having excellent features like a very good electron/hole conductor, easily tunable band-gap and availability at nanoscale in numerous shapes, ZnO based photo anodes suffer from the instability due to photo-degradation and corrosion at higher/alkaline pH conditions.²⁷⁻²⁹ Moreover, the presence of intrinsic defects at ZnO surface and $\text{Zn}(\text{OH})_2$ layer (especially in case of solution grown nanowires) is responsible for electron trapping and hence poor photo conversion efficiency.³⁰⁻³² While, in comparison to bare ZnO, surface functionalization not only offers a minimized contact of ZnO layer with electrolyte solution (enhanced stability) but provides an effective separation of holes from the ZnO surface. In addition to these two advantages, surface functionalized nanowire films³³⁻³⁶ (e.g. hybrid nanowire films, ZnO/Ag nanostructured films, Au/Ag embedded ZnO films, metallic SWCNT-ZnO composite or Au-ZnO flower-rod

*Department of Physics and**National Center for Photovoltaic Research and Education (NCPRE),**Indian Institute of Technology Bombay, Powai, Mumbai-400076, India.***Email:m.aslam@iitb.ac.in, Phone: +91-22-2576-7585*

heterostructure etc.) show an improved electrical conductivity. Thus, realization of 'ITO/FTO free photoanode' can be aimed in which hybrid film has two roles one as photo active layer for catalytic activity and second as an efficient transport medium for photo-generated charge carriers.³⁷ In yet another scheme, Al-doped and hydrogen annealed ZnO nanowires have also been proposed as TCO (transparent conducting oxide) free efficient water splitting photoanodes.³⁸ Though, ITO/FTO free ZnO nanowire based photoanodes are reported, but studies are very limited and not well explored for water splitting performance.^{39,40-41}

This report presents a facile process to get size controlled gold nanoparticle (in range of 5 nm to 30 nm) functionalized photoactive nanowire electrodes (purple to green color films) by annealing gold sputtered ZnO nanowire films. An enhanced band edge emission and fully suppressed defect emission is observed due to excitonic-plasmonic coupling between ZnO NW and AuNPs. Gold nanoparticle has multiple roles such as (i) it acts as light designer in ZnO nanowire photoanodes and increases visible light absorption due to localized surface plasmons. (ii) Interaction of localized electric field of AuNP with ZnO surface generates electron-hole pairs near the nanowire surface which can be separated effectively due to the surface barrier. The photo excited electrons (plasmons) of AuNPs stay at higher energy state and are easily transferred to the ZnO conduction band (AuNPs: as electron donor). (iii) Surface capping by thin AuNPs layer reduces surface traps /defects and minimizes the holes trapping in ZnO valence band (efficient charge separation). Near conformal covering (with AuNPs of average 6 nm size) of ZnO nanowire photoanode shows around two orders of increase in electrical conductivity and 30 times enhanced water splitting efficiency as compared to pristine defect ridden ZnO photoanode.

2. Experimental and characterization techniques

ZnO nanowires were grown on amorphous glass substrates using low temperature hydrothermal growth.⁴⁵ Glass slides were cleaned using soap solution followed by ultrasonication in DI water, acetone and isopropyl alcohol. Cleaned substrates were then functionalized using colloidal solution of zinc sol via dip coating followed by annealing at 400°C in air atmosphere for 1 hour. ZnO seeded substrate kept into sealed glass bottle which contains 50 mM aqueous solution of zinc nitrate hexahydrate [Sigma-Aldrich, 99% purity] and hexamine (HMT) [Sigma-Aldrich, 99% purity], 1:1 mole ratio. Growth reaction was carried out in the laboratory oven at fixed temperature (90 °C) for 12 hour.⁴² Finally, ZnO nanowire grown substrates were naturally cooled to room temperature and cleaned using DI water and ethanol. A 15 nm thick gold layer was sputtered over hydrothermally grown ZnO nanowire films using NORDIKO metal sputtering system. A programmable split type tube furnace was used to anneal the ZnO: Au nanowire films at 200, 400 and 600 °C under argon atmosphere. The annealing at different temperatures revealed different size gold nanoparticles (5 nm to 30 nm) on ZnO nanowire surface.

Morphological characterizations of gold coated ZnO nanowire were carried out by JEOL JSM-7600F FEG- Scanning Electron Microscopy (HRSEM) operated at 15kV. Xpert PANALytic x-ray

diffractometer (XRD) was utilized for the crystallographic investigations. Lattice fringes and SAED pattern was recorded using HRTEM (JEOL JEM 2100F), field emission gun transmission electron microscope at an accelerating voltage of 200 kV. Elemental mapping of core-shell nanowire was carried out using STEM mode of HRTEM. Optical transmittance was taken using Lambda 950 (Perkin Elmer) in range 300-800 nm at room temperature with integrating sphere assembly. PL measurement was performed using He-Cd laser with 325 nm excitation wavelength.

Three-electrode based photoelectrochemical measurements were performed using Autolab potentiostat/galvanostat. Gold nanoparticles functionalized ZnO nanowire films were used as working electrode (photoanode), Pt wire as counter and Ag-AgCl as reference electrode in 0.5M Na₂SO₄ electrolyte solution. The photoanodes were illuminated by Xenon lamp (100 mW/cm²) at 1cm² area for photoelectrical measurements. Visible light sensitivity of Au-ZnO NWs photoanode was measured at 500 mV fixed bias with respect to Ag-AgCl reference electrode. Linear sweep voltammetry measurements were performed to estimate water splitting performance of gold nanoparticles decorated ZnO nanowire films. Time dependent photocurrent (amperometry) measurements under visible light excitation were carried out for one hour to test the stability of AuNPs coated ZnO NWs photoanodes. All the photoanodes were prepared on non-conducting (ITO/FTO free) glass substrates. Four different electrodes named as ZnO_ASG (as-grown ZnO nanowire), Au_15nm (15 nm gold sputtered ZnO nanowire), Au_200 °C (gold sputtered ZnO nanowire annealed at 200 °C), Au_400 °C (gold sputtered ZnO nanowire annealed at 400 °C) and Au_600 °C (gold sputtered ZnO nanowire annealed at 600 °C) were tested for PEC water splitting. AuNPs functionalization of ZnO NWs via sputtering is a clean process and does not apply reducing or stabilizing agents, thus, there is no contamination issues from hydrocarbons which is typically a big concern during soft chemical processing.⁴³ In addition, the gold nanoparticles are directly attached to the ZnO nanowire surface without any intermediate surface ligands/binders which makes it more favorable for photo-catalytic activity.

3. Results and discussion

3.1 Morphological and structural properties

Large area tilt view SEM images of as-sputtered and post annealed Au-ZnO NW films are shown as Fig.1a-1d. As-sputtered gold conformally covers the entire surface of the NWs (Fig.1a), while the annealing at 200 °C results in aggregation of small sized Au nanoparticles which are distributed all along the length of the NW. The annealing at 400 °C results in aggregation of irregular shape and larger size gold nanoparticles (Fig.1c) and exposes a partially covered ZnO NW surface. The 600 °C annealing further increases the size of gold nanoparticles and results into a larger uncovered ZnO nanowire surface (Fig.1d). Top view SEM image of AuNP coated single nanowire (Fig.1e – 1h) shows that sputtered gold does not aggregate till 200 °C and the top hexagonal facet of nanowire remains fully flat or conformally covered with very small sized nanoparticles. After annealing at 400 °C, gold agglomerates into arbitrary shaped big-

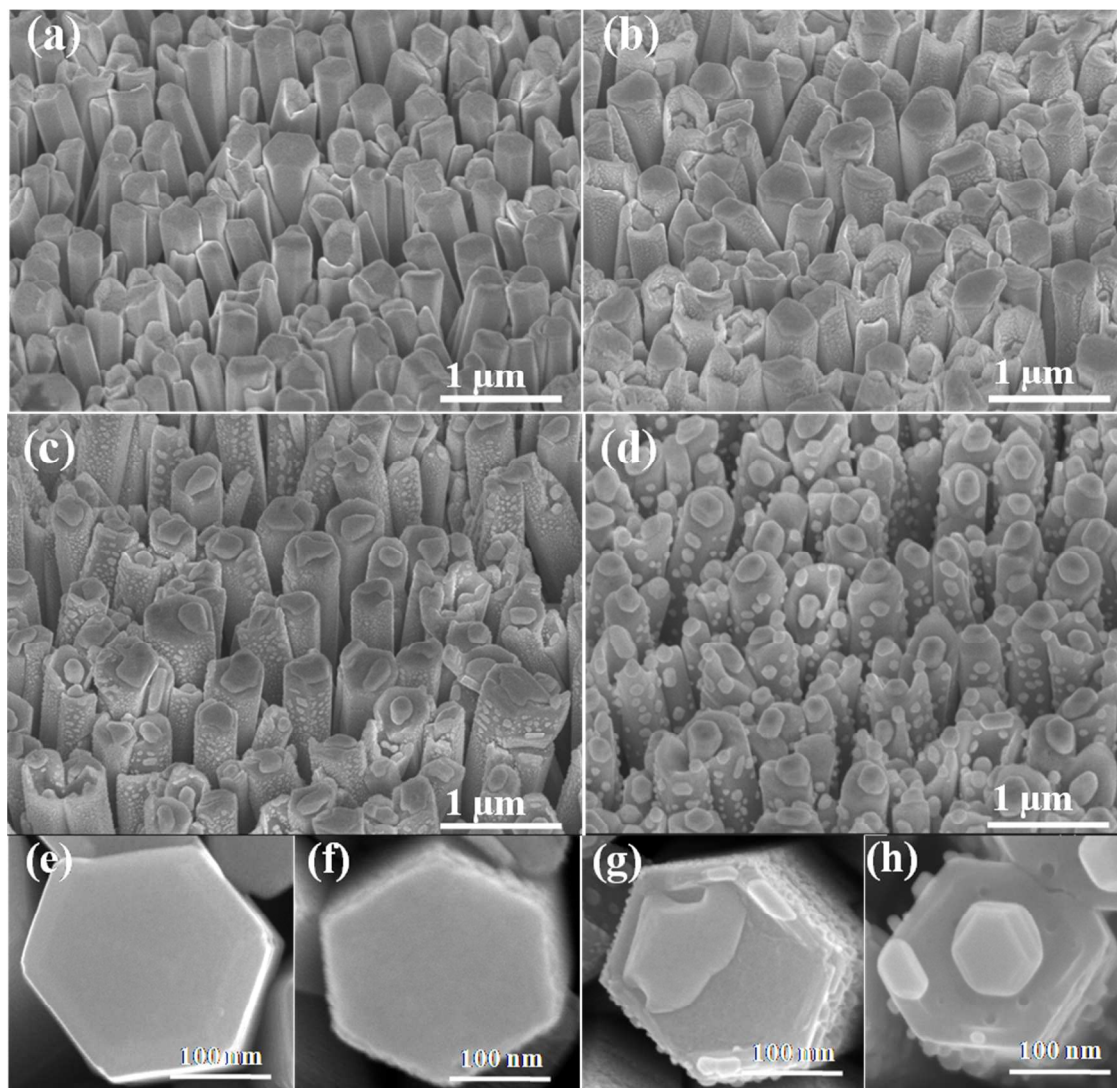


Fig.1 Scanning electron microscopic images of gold nanoparticle functionalized ZnO nanowires. (a) As sputtered gold layer (15 nm) over ZnO nanowire film, (b) Au-ZnO nanowire film annealed at 200 °C, (c) 400 °C and (d) 600 °C, respectively. SEM image of single Au-ZnO nanowire (e) as sputtered gold layer, (f) annealed at 200 °C, (g) 400 °C, and (h) 600 °C, respectively.

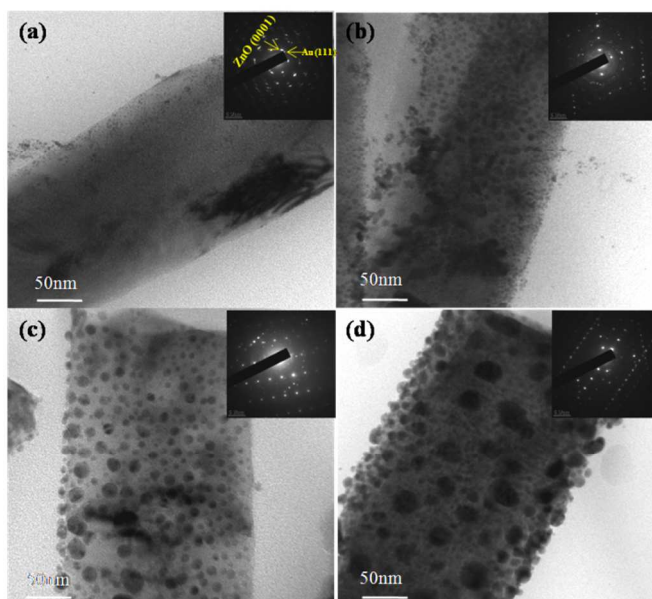


Fig.2 High resolution TEM images of (a) as-sputtered gold layer over ZnO nanowire, (b) Au-ZnO nanowire annealed at 200 °C, (c) 400 °C and (d) 600 °C, respectively. Inset of all the images show selected area diffraction pattern of respective samples.

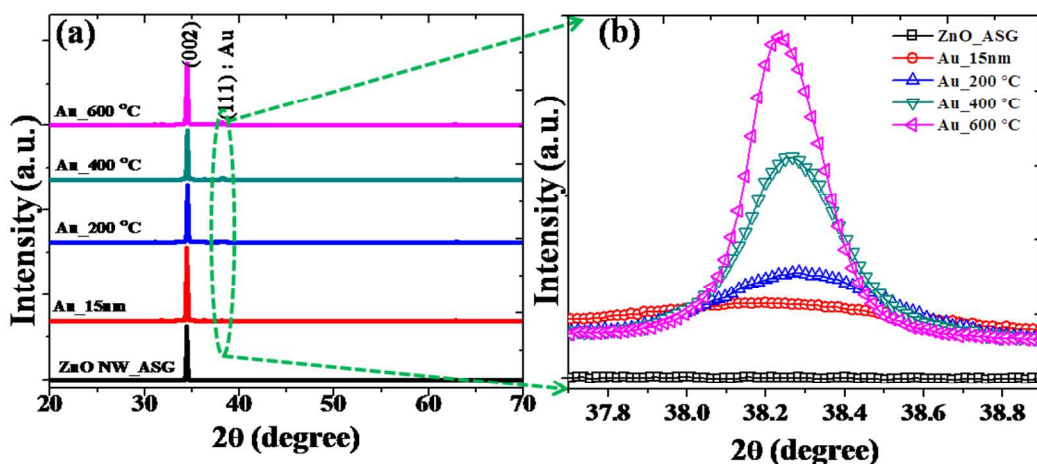


Fig.3 (a) XRD spectra of as-grown and gold coated ZnO nanowire films annealed at different temperatures as labelled in the figure. (b) Short range XRD scan of different size gold nanoparticles decorated nanowire films as indicated.

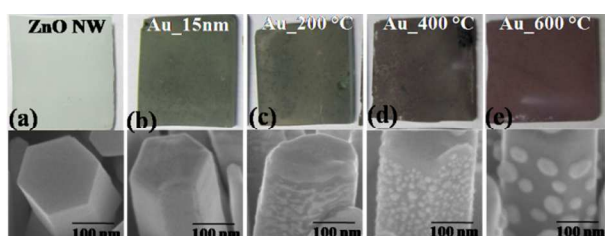


Fig.4 Digital photograph of pristine ZnO, gold as-sputtered ZnO NWs film and Au-ZnO NWs films annealed at different temperature (200, 400 and 600 °C) associated with single nanowire SEM images. Size dependent plasmonic effect of gold nanoparticles renders different color of Au-ZnO nanowire films.

size nanoparticles (Fig. 1g) while hexagonal disks are formed for 600 °C (Fig. 1h). Since amount of sputtered gold is equal in all the samples, hence density of nanoparticles decreases as the Au nanoparticle size increase at higher annealing temperature. The samples annealed at 600 °C shows the lowest density of NPs due to larger aggregation and results into larger exposed/open surface area of ZnO NWs.

Fig.2 shows HRTEM images of single ZnO nanowire coated with gold nanoparticles. The as-sputtered gold fully covers the ZnO nanowire surface (Fig.2a) and annealing of these films at 200 °C results in 5-10 nm size gold nanoparticles (Fig.2b). An increase in annealing temperature to 400 °C results an increase of gold nanoparticles size (10- 20 nm) as shown in Fig.2c and further increase in annealing temperature to 600 °C shows the largest size particles (Fig.2d) with size distribution of 10-30 nm. The density of nanoparticles appears to be lowered due to agglomeration (Fig.2d) at higher temperature. SAED pattern of as-sputtered gold ZnO nanowire (inset Fig.2a) has both circles and periodic points, which indicated the hybrid Au-ZnO structure formation. Similar SAED pattern is also observed for Au-ZnO samples annealed at 200 °C, however, periodic points are more distinguished and clear for 400 and 600 °C annealed samples, due to larger sized well-separated AuNPs.

XRD spectra of as-grown ZnO nanowires and gold coated nanowires (Fig.3a) shows that all nanowire films are highly

oriented towards (002) direction and have wurtzite crystal structure (JCPDS No. 36-1451). Gold coating results in appearance of an additional peak in XRD spectrum (along with standard ZnO peaks) at 38.1° 2θ value which corresponds to Au (111) peak.⁴⁴ The intensity of the gold peak is lowest due to thin and uniform as-sputtered layer which remains similar for 200 °C annealed Au-ZnO nanowires. The aggregation and formation of large Au islands (400 and 600 °C) at the top as well as side facets of the ZnO surface results an increase in the intensity of the gold peak (Fig.3b).

3.2 Optical properties of Au functionalized ZnO nanowire films

The varied size of gold nanoparticles shows size dependent plasmonic properties, which is directly visible as varied colors of the Au-ZnO nanowire films (Fig.4).⁴⁶⁻⁴⁷ The pristine NW film without gold NPs (as-grown nanowires) shows cream-white color, while as-sputtered (Au_15 nm) Au-ZnO NWs film is green-golden in color. The 200 °C annealed Au-ZnO film is golden yellow in color, while 400 °C and 600 °C annealed samples are light red and dark red in color, respectively. This change in color after annealing (due to size dependent plasmonic properties of Au nanoparticles) reflected as variation in visible

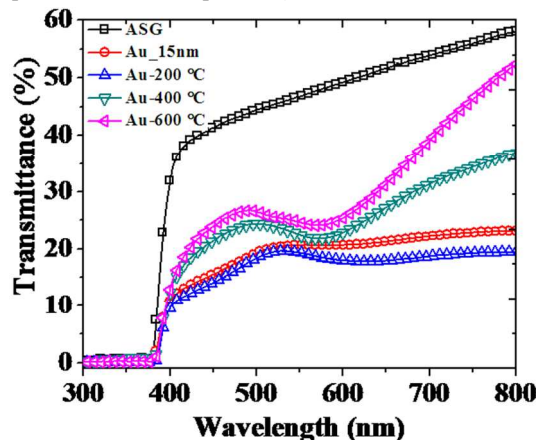


Fig.5 Transmittance spectra of different size gold nanoparticles functionalized ZnO nanowire films.

light absorption properties with an increase in size of Au particles on ZnO NW surface.⁴⁷ Transmittance spectra of Au-ZnO NWs film is recorded and found that 200 °C annealed NWs shows minimum transmittance (Fig.5), while 600 °C annealed Au-ZnO NWs films show highest transmittance as well as strong surface plasmon around 580 nm. In comparison to bigger size AuNPs, approximately 10% decrease in transmittance is observed for small size and dense AuNP functionalized nanowire films (as-sputtered and 200 °C). A dense covering of nanoparticles causes an effective excitonic-plasmonic coupling or an excellent photon trapping effect leads to an enhanced broad range absorption (500-700 nm) as has been reported for Au-TiO₂, Au-Fe₂O₃ functionalized nanorods.^{16,18,48,49} Thus, gold functionalization increases visible light absorption which is beneficial and a primary requirement for more efficient photoanode to water splitting application.^{16,18,26,50}

3.3 Correlation of emission and electrical characteristics

The room temperature PL measurement of Au-ZnO nanowire films are given in Fig.6. The as-grown ZnO nanowires films show intense defect emission. The intensity of defect band emission reduces after annealing and is fully suppressed when annealed at 200 °C. However, higher annealing temperature (400 & 600 °C) shows an increase in defect emission intensity with a red shift in the peak position. The ambiguous nature of the defect

band is further analyzed by de-convoluting defect band into three Gaussian peaks⁵¹ related to green (P₁), yellow (P₂) and red color (P₃) emissions (Fig.6b – 6f). The cause of green emission in ZnO is highly controversial, however, presence of singly charged oxygen vacancies and other surface species has been considered a cause in solution grown ZnO nanowires.⁵¹ While yellow and red emissions correspond to doubly charge oxygen vacancies and excess of oxygen or lattice strain, respectively. Green emission is the highest in as-grown nanowires which get almost fully suppressed after AuNPs coating followed by annealing at 200 °C (Fig.6b and Fig.6c). To study the relative change in defect emission for different size AuNPs coated ZnO nanowire films, the change in intensity ratio of defect emission with respect to band edge emission is calculated. Fig.7a represents a comparative change in intensity of green emission (I_{P1}) and red emission (I_{P3}) emission with respect to band edge emission (I_{UV}) of all the samples. Relative intensity of green emission (I_{P1}/I_{UV} = 0.8) is highest for as-grown nanowire. Gold NPs coating reduces intensity ratio of green emission (I_{P1}/I_{UV} = 0.18, for as-sputtered gold) and 200 °C annealed samples show minimum green emission (I_{P1}/I_{UV} = 0.05). The intensity of red emission is initially slowly decreases for as-sputtered and 200 °C annealed samples. While annealing at 400 °C and 600 °C results increase in the intensity of red emission. An increase in red emission can be corresponds to the lattice strain which occurs due to the diffusion

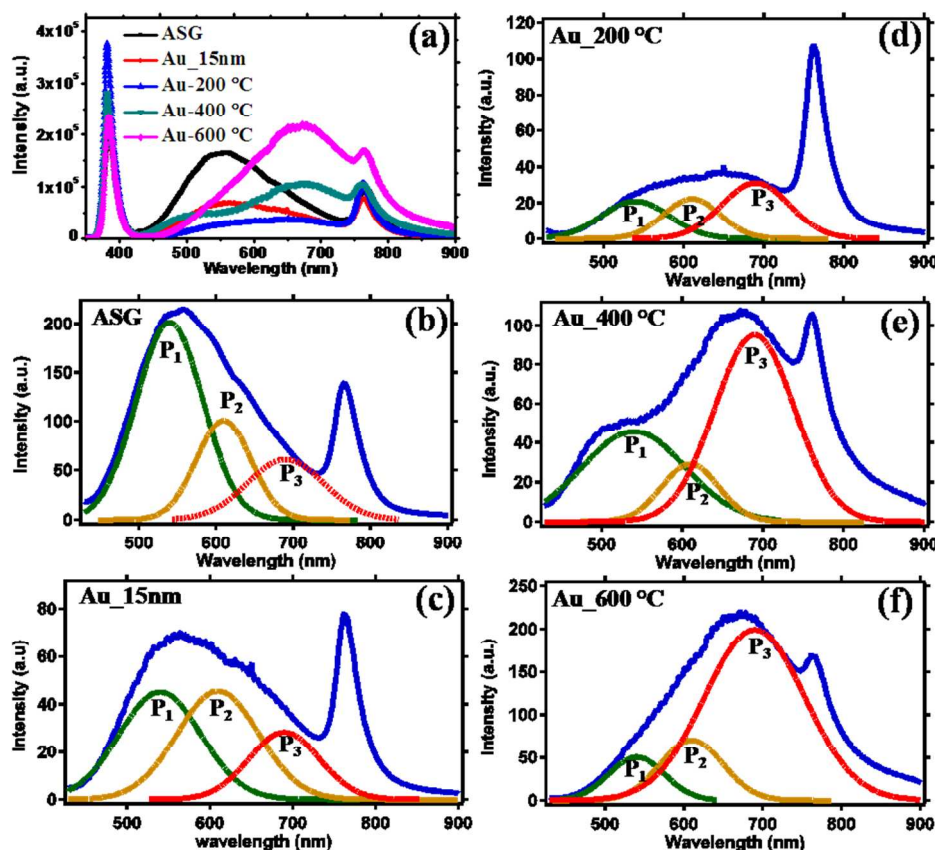


Fig.6 (a) Room temperature PL measurements of gold nanoparticles decorated ZnO nanowire films. Three Gaussian peaks fitting of defect band emission (b-f) for as-grown nanowires and size dependent gold nanoparticles decorated nanowire films annealed at different temperatures as labeled (The sharp peak around 764 nm is the second harmonic peak of the band edge emission).

of gold at higher temperature. A lattice strain changes the crystal symmetry of ZnO and cause lattice distortion leading to creation of new defects states at near-band edge.⁵² A thermally driven defect formation has been reported at gold-ZnO interface, which has shown a new emission at 2 eV (red emission) after annealing of Au-ZnO films at 650 °C.⁵³ Excess oxygen or oxygen interstitial formation is also responsible for an increase in red emission which appears at higher temperature annealing.^{54,55} The transfer of photoexcited electrons (due to surface plasmon resonance) from AuNPs to the conduction band of ZnO is responsible for the enhancement in the band edge emission after AuNPs functionalization.^{54,56,57} The strong coupling between surface plasmon and exciton is considered as cause for increases in the density of states and enrich the intensity of spontaneous emission in the ZnO nanorods.⁵⁸ An enhancement in near-band edge emission has been seen due to surface plasmon resonance when ZnO nanobelts is coated with gold nanoparticles.⁵⁹ On the other-hand, the transfer of electrons from defect levels of ZnO to the Fermi level of gold NPs leads to suppression in defect emission.¹⁵ Furthermore, since surface adsorbed oxygen and other surface states are covered with the gold nanoparticles, hence, a well-controlled and nearly fully suppressed defect emission of ZnO nanowires is observed. To investigate the role of defects in electrical transport properties of ZnO: Au NWs films, current-voltage characteristics is measured under dark condition (Fig.7b). An increased electrical conductance by an order is observed for as-sputtered gold sample.

As compared to as-grown ZnO nanowire, approximately two orders of enhancement in electrical conductance is observed for 200 °C annealed samples. Reduction of surface defects and improved interconnects between NWs through gold nanoparticles is the main cause for enhanced electrical conduction. As-sputtered Au-ZnO films have a depletion layer (adsorbed oxygen) between AuNP and NWs surfaces, which gets removed after annealing at 200 °C and results in further enhanced electrical conduction^{55,58} Annealing at 400 °C and 600 °C also shows an improved electrical conductivity though they have higher concentration of red emission related defects. Thus, it can be considered that presence of green emission related defects such as surface adsorbed oxygen and singly charged oxygen vacancies are mainly responsible for poor electrical conductivity

in these nanowire films.⁶⁴ Gold nanoparticles functionalization reduces surface traps and enhances electrical conductivity in ZnO nanowires films. This indicates an effective charge separation and collection than the pristine ZnO nanowire based anodes.

3.4 Photoelectrochemical water splitting characteristics of ITO/FTO free Au-ZnO NWs anode

The time dependent photocurrent measurements (*I-t* plot) of Au-ZnO NWs anode are performed under visible light ON/OFF conditions at a fixed external bias (0.5 V /Ag-AgCl). As-grown ZnO nanowires show a sharp change (an order) in current under visible light illumination (18 μA) photocurrent, while 200 °C annealed Au-ZnO NWs show highest value of photocurrent (115 μA) among all the photoanodes (Fig.8a). Under visible light illumination, the surface plasmon resonance of AuNPs excites electrons and supplies to ZnO nanowires continuously. For 200 °C annealed samples, the density of AuNPs is higher and small in size; hence, intense surface plasmon resonance (SPR) occurs and causes a continuous supply of large number of electrons to nanowire system that leads to highest photocurrent with unsaturated value. Au-ZnO NWs annealed at higher temperature have large size and less populated gold nanoparticles that lead to less intense surface plasmon. Therefore, less number of photo-excited electron transfers from gold nanoparticles to ZnO nanowire and photocurrent gets saturated faster with lower value.

The linear sweep voltammograms shows highest photocurrent density (300 μA/cm²) for Au-ZnO nanowire anodes annealed at 200 °C (Fig.8b). Relatively lesser value of photocurrent densities, 140 μA/cm² and 85 μA/cm² are measured for 400 °C and 600 °C annealed Au-ZnO nanowire films at 1V bias with respect to Ag-AgCl reference electrode. Presence of annealing induced defects and lower plasmon-exciton interaction [lower density of large size (20-30 nm) gold nanoparticles] are the possible causes for lower photocurrent density in high temperature annealed (400 and 600 °C) NW. The plasmon-exciton coupling strongly depends upon the metal nanoparticles size and formation of resonant state under light irradiation results in an enhancement of local electric field at Au-ZnO interface.⁶⁵ This leads to an increase in the light absorption and rapidly creates electron-hole pairs at the surface which directly contributes to photocurrent.⁶⁶ The size, structure and density of gold nanoparticles effectively control the light

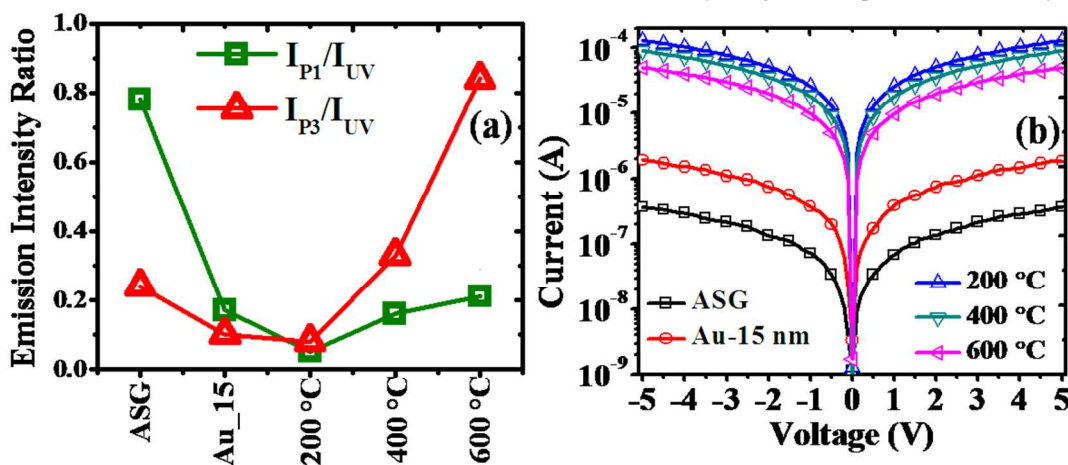


Fig.7(a) Variation of relative intensity of red and green emissions with respect to temperature. (b) Current-voltage plot of as-grown and annealed AuNP decorated ZnO nanowire films.

absorption and electron-hole pair generation. Since, coating of large size AuNPs leads to higher open surface of ZnO and lower density of AuNPs which renders poor plasmon-exciton interaction and result in lower photocurrent density. The 200 °C annealed sample reveals an intense plasmon-exciton interaction due to small size and large density (fully capped ZnO surface) of AuNPs with respect to as-sputter gold sample. However, formation of larger size gold nanoparticles leads to lower density in case of high temperature annealed samples (400 and 600 °C) which is responsible for reduction in plasmon-exciton interaction.

Various hybrid structures such as hierarchical Au-ZnO flower-rod heterostructures⁶⁷, patterned AuNPs/ZnO nanowires¹⁸ and plasmonic Ag/ZnO embedded nanostructures⁶⁸ have been proposed as photoanodes which show 120, 350, and 800 $\mu\text{A}/\text{cm}^2$ photocurrent, respectively. However, above mentioned photoanodes were designed on FTO (conducting glass) substrates, while photoanodes presented in our work are fabricated on non-conducting glass substrates. The value of photocurrent found in this work is almost in the same range as reported in the literature though we used ITO/FTO free glass substrate which makes our photoanodes significantly different and important for water splitting activity.³⁸

The efficiency of solar driven hydrogen generation is calculated using following formula.⁶⁹

$$\eta(\%) = \frac{J_p(1.23 - V)}{L_{\text{light}}} \times 100$$

Where J_p is the photocurrent density (mA/cm^2), V (volt) is applied voltage and J_{light} (mW/cm^2) is the power of incident light. The efficiency of as-grown ZnO nanowire film is found to be 0.012% at 0.6V (vs. Ag/AgCl) which increases to 0.13% for AuNP functionalized ZnO (200 °C annealed) electrode (Fig.8c). Thus, ZnO nanowire films functionalized with small size gold nanoparticles show nearly 30 times increase in photoelectrochemical water splitting efficiency in comparison to pristine ZnO NWs. The stability of Au-ZnO photoanode against photo corrosion and degradation is also tested through long term photocurrent measurements. Fig.8d indicates that 200 °C and 400 °C annealed NWs show minimum variation/fluctuation in photocurrent for one hour continuous measurement. As-grown nanowires and 600 °C annealed NWs samples show relatively lesser stability in photocurrent due to direct contact of large area of ZnO surface with the electrolyte.

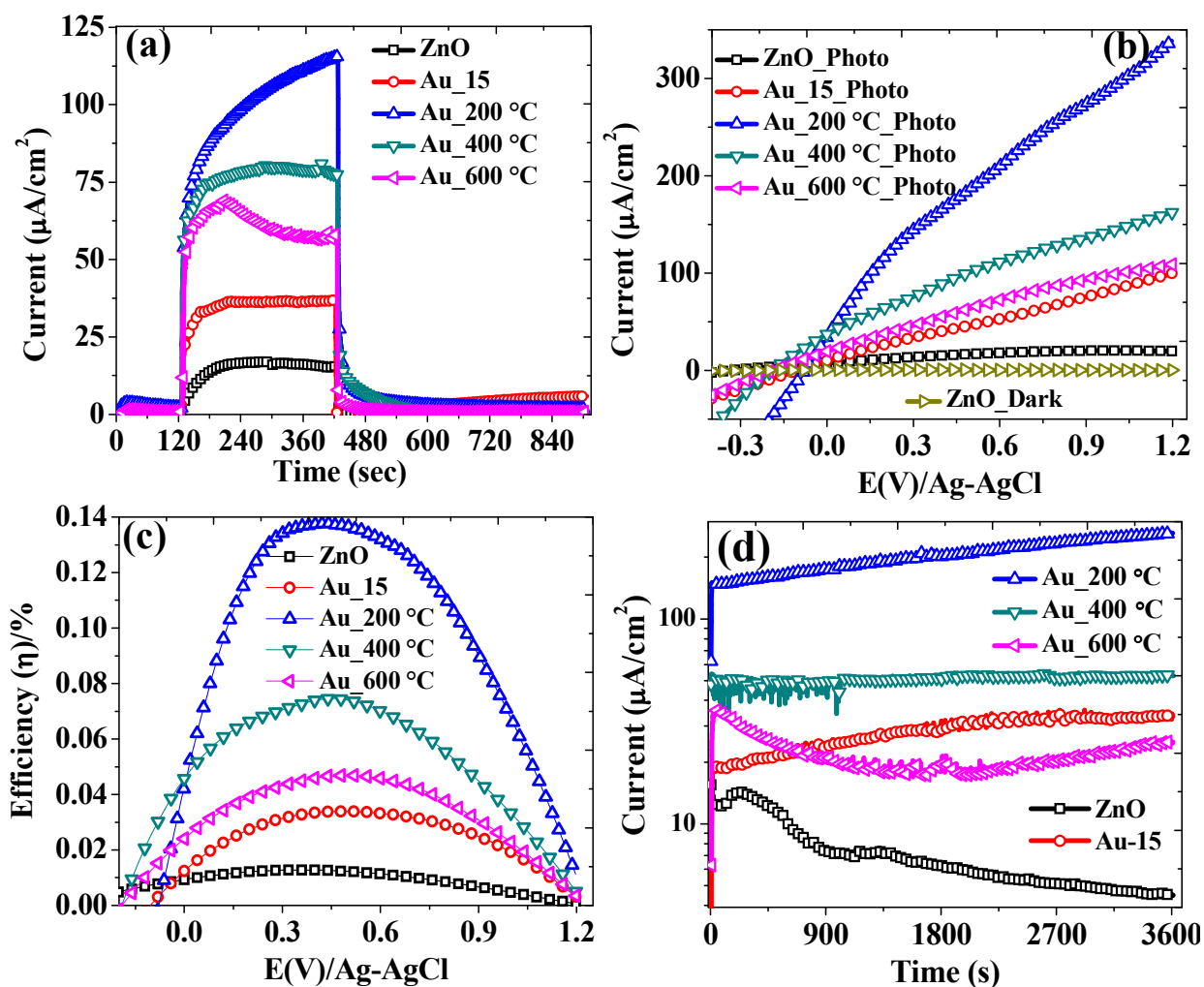


Fig. 8 (a) Time dependent photoresponse of AuNP functionalized ZnO nanowires, (b) linear voltammetric scans of as-grown ZnO NWs and size dependent gold nanoparticle coated ZnO nanowire photoanodes. (c) Solar to hydrogen conversion efficiency of Au-ZnO NWs photoanode and (d) stability test of photoanode for one hour measurement time.

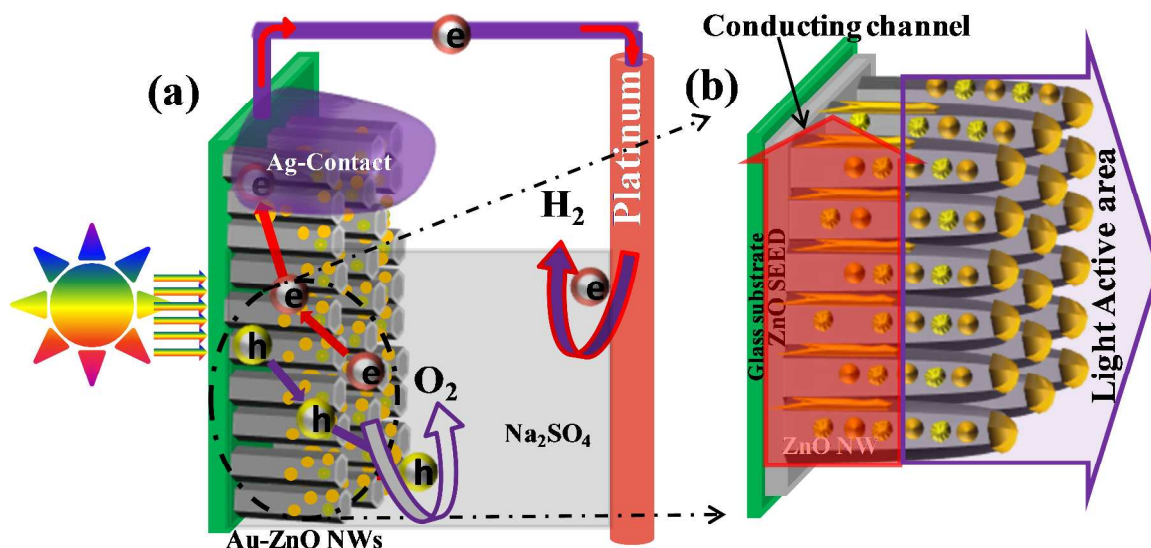


Fig.9 Schematic Diagram (a) Photoelectrochemical water splitting process in Au-ZnO NWs anodes and (b) Zoom in portion of anode: conducting channel for electrons transport and light active area for photocatalytic activity.

Fig.9 presents a schematic diagram of water splitting process in Au-ZnO nanowire anode. Herein, Au-ZnO nanowire film itself acts as a conducting substrate for the electron transport and a bottom dense layer comprising ZnO NWs and gold-interconnects between nanowires takes part in electrical conduction. The open surface of gold functionalized ZnO NWs behaves as light active center for photocatalytic activity in which gold nanoparticles take part as light sensitizer. Under visible light irradiation, formation of plasmons at gold nanoparticles surface produces intense localized electric field at the Au-ZnO interface.²⁰ The interaction of localized electric field of AuNP with ZnO surface generates electron-hole pairs near the nanowire surface.³⁵ These photoexcited electrons of AuNPs stay in higher energetic state and thus could be easily transferred to the ZnO conduction band causing an enhanced photocurrent.⁷⁰ Interestingly, formation of a Schottky barrier (the higher work function of gold than the electron affinity of ZnO) at Au-ZnO interface prevents transfer of photo-generated electrons towards electrolyte.²³ In addition to this, surface defects/traps of ZnO NWs are passivated by AuNPs which reduces the holes trapping and ultimately improves the photo-charge separation and thus, the overall performance of photoelectrochemical cell is improved. Thus, AuNPs act as light absorber as well as electron donor in functionalized ZnO nanowire anode leading to an enhanced stable photocurrent and can serve as a new nanostructured photoanode for fabrication of low cost and facile energy conversion device.

Conclusions

Sputtering of gold layer over ZnO nanowire film followed by annealing gives size controlled AuNP functionalized ZnO nanowire films. Densely packed ZnO nanowire films with small size AuNPs shows enhanced band edge emission and fully suppressed defect emission leading to two orders of enhancement in electrical conductivity. The 30 times enhanced photocurrent and 0.13% water splitting efficiency are observed in gold nanoparticle surface functionalized ZnO nanowire films. The improved efficiency and enhanced stability could be attributed to

improvements in photoanode by 'multifunctional' gold nanoparticles. First, the interaction of localized electric field (due to SPR) of AuNPs with ZnO surface increases the visible light absorption and creates larger number of electron-hole pairs near the nanowire surface. Second, passivation of surface defects/traps of ZnO reduce holes trapping which leads to improved water splitting characteristics of ITO/FTO free anodes.

Acknowledgement

We acknowledge IRCC, IIT Bombay (seed grant) and National Centre for Photovoltaic Research and Education (NCPRE), IIT Bombay (funded through Ministry of New and Renewable Energy, Government of India) for the financial support. Authors are also grateful to Professor Dinesh Kabra, Department of Physics, IIT Bombay for helpful discussions on optical properties.

References

1. X. Yang, A. Wolcott, G. Wang, A. Sobo, R. C. Fitzmorris, F. Qian, J. Z. Zhang, and Y. Li, *Nano Lett.*, 2009, **9**, 2331.
2. A. Wolcott, W. Smith, T. R. Kuykendall, Y. Zhao, and J. Z. Zhang, *Adv. Funct. Mater.*, 2009, **19**, 1849.
3. Y. Wang, Q. Wang, X. Zhan, F. Wang, and M. Safdar, *Nanoscale*, 2013, **5**, 8326.
4. Z. Li, W. Luo, M. Zhang, J. Feng, and Z. Zou, *Energy Environ. Sci.*, 2013, **6**, 347.
5. Y. Myung, D. M. Jang, T. K. Sung, Y. J. Sohn, G. B. Jung, Y. J. Cho, H. S. Kim, and J. Park, *ACS Nano*, 2010, **4**, 3789.
6. Y. Tak, H. Kim, D. Lee, and K. Yong, *Chem. Commun.*, 2008, 4585.
7. S. Jung and K. Yong, *Chem. Commun.*, 2011, **47**, 2643.
8. Y. Liu, Z. H. Kang, Z. H. Chen, I. Shafiq, J. A. Zapien, and I. Bello, *Cryst. Growth Des.*, 2009, **9**, 3222.
9. G. Kwak, M. Seol, Y. Tak, and K. Yong, *J Phys. Chem. C*, 2009, **113**, 1208.
10. Y. Zhang, Z. Wu, J. Zheng, X. Lin, H. Zhan, S. Li, J. Kang, J. Bleuse, and H. Mariette, *Sol. Energy Mater. Sol. Cells*, 2012, **102**, 15.
11. H. Li, C. Cheng, X. Li, J. Liu, C. Guan, and Y. Y. Tay, *J. Phys. Chem. C*, 2012, **116**, 3802.
12. C. Y. Chen, C. Lin, M. J. Chen, G. R. Lin, and J. H. He, *Nanotechnology*, 2009, **20**, 185605.

13. A. Kushwaha and M. Aslam, *Electrochimica Acta*, 2014, **130**, 222.
14. C. H. Kim, Y. C. Park, J. Lee, W. S. Shin, S.J. Moon, J. Park, and J. Kim, *Mater. Lett.*, 2011, **65**, 1548.
15. A. Bera and D. Basak, *Nanotechnology*, 2011, **22**, 265501.
16. E. Thimsen, F. Le Formal, M. Grätzel, and S. C. Warren, *Nano Lett.*, 2011, **11**, 35.
17. G. Rahman and O.-S. Joo, *Mater. Chem. Phys.*, 2013, **140**, 316.
18. P. Thiyagarajan, H.J. Ahn, J.S. Lee, J.C. Yoon, and J.H. Jang, *Small*, 2013, **9**, 2341.
19. F. Wu, X. Hu, J. Fan, E. Liu, T. Sun, L. Kang, W. Hou, C. Zhu, and H. Liu, *Plasmonics*, 2012, **8**, 501.
20. D. B. Ingram and S. Linic, *J. Am. Chem. Soc.*, 2011, **133**, 5202.
21. Y.C. Pu, G. Wang, K.D. Chang, Y. Ling, Y.K. Lin, B. C. Fitzmorris, C.M. Liu, X. Lu, Y. Tong, J. Z. Zhang, Y.J. Hsu, and Y. Li, *Nano Lett.*, 2013, **13**, 3817.
22. W.J. An, W.N. Wang, B. Ramalingam, S. Mukherjee, B. Daubayev, S. Gangopadhyay, and P. Biswas, *Langmuir*, 2012, **28**, 7528.
23. T. Bora, H. H. Kyaw, S. Sarkar, S. K. Pal, and J. Dutta, *Beilstein J. Nanotechnol.*, 2011, **2**, 681.
24. Y. Zhang, J. Xu, P. Xu, Y. Zhu, X. Chen, and W. Yu, *Nanotechnology*, 2010, **21**, 285501.
25. S. Link and M. El-Sayed, *J. Phys. Chem. B*, 1999, **103**, 4212.
26. W. L. Ong, S. Natarajan, B. Kloostera, and G. W. Ho, *Nanoscale*, 2013, **5**, 5568.
27. J. Zhou, N. S. Xu, and Z. L. Wang, *Adv. Mater.*, 2006, **18**, 2432.
28. J. Domenech, *J Phys Chem C*, 1986, **397**, 1123.
29. M. Liu, C.Y. Nam, C. T. Black, J. Kamcev, and L. Zhang, *J. Phys. Chem. C*, 2013, **117**, 13396.
30. D. C. Iza, D. Muñoz-Rojas, Q. Jia, B. Swartzentruber, and J. L. Macmanus-Driscoll, *Nanoscale Res. Lett.*, 2012, **7**, 655.
31. A. Layek, B. Manna, and A. Chowdhury, *Chem. Phys. Lett.*, 2012, **539-540**, 133.
32. X. Bai, L. Wang, R. Zong, Y. Lv, Y. Sun, and Y. Zhu, *Langmuir*, 2013, **29**, 3097.
33. H. Ishiguro, in *Optics Info Base*, 2012, p. <http://dx.doi.org/10.1364/FIO.2012.FTh1A.6>.
34. Y. R. Park, N. Liu, and C. J. Lee, *Curr. Appl. Phys.*, 2013, **13**, 2026.
35. S. Linic, P. Christopher, and D. B. Ingram, *Nat. Mater.*, 2011, **10**, 911.
36. S. Mehra, M. G. Christoforo, P. Peumans, and A. Salleo, *Nanoscale*, 2013, **5**, 4400.
37. A. Kushwaha and M. Aslam, *J. Phys. D: Appl. Phys.*, 2013, **46**, 485104.
38. C.H. Hsu and D. H. Chen, *Nanoscale Res. Lett.*, 2012, **7**, 593.
39. S.G. Ihn, K.S. Shin, M.J. Jin, X. Bulliard, S. Yun, Y. Suk Choi, Y. Kim, J.H. Park, M. Sim, M. Kim, K. Cho, T. Sang Kim, D. Choi, J.Y. Choi, W. Choi, and S. W. Kim, *Sol. Energy Mater. Sol. Cells*, 2011, **95**, 1610.
40. D. H. Kim, J. H. Heo, D. J. Kwak, and Y. M. Sung, *J. Electr. Eng. Technol.*, 2010, **5**, 1460.
41. C.H. Hsu and D. H. Chen, *Int. J. Hydrogen Energy*, 2011, **36**, 15538.
42. A. Kushwaha and M. Aslam, *Int. J. Nanoscience*, 2011, **10**, 635.
43. E. Vanecht, K. Binnemans, J. W. Seo, L. Stappers, and J. Fransaer, *Phys. Chem. Chem. Phys.*, 2011, **13**, 13565.
44. I. Dutta, C. B. Munns, and G. Dutta, *Thin Solid Films*, 1997, **304**, 229.
45. K. Ai, Y. Liu, and L. Lu, *J. Am. Chem. Soc.*, 2009, **131**, 9496.
46. S. K. Ghosh and T. Pal, *Chem. Rev.*, 2007, **107**, 4797.
47. I. V. Kityk, K. J. Plucinski, J. Ebothé, A. Umar, and M. Oyama, *J. Appl. Phys.*, 2005, **98**, 084304.
48. K. Kim, P. Thiyagarajan, H. J. Ahn, S.I. Kim, and J.H. Jang, *Nanoscale*, 2013, **5**, 6254.
49. T. El-Brolossy, T. Abdallah, M. B. Mohamed, S. Abdallah, K. Easawi, S. Negm, and H. Talaat, *Eur. Phys. J. Spec. Top.*, 2008, **153**, 361.
50. D. M. Schaadt, B. Feng, and E. T. Yu, *Appl. Phys. Lett.*, 2005, **86**, 063106.
51. A. Kushwaha and M. Aslam, *J. Appl. Phys.*, 2012, **112**, 054316.
52. Y. Zhao, M. Zhou, Z. Li, Z. Lv, X. Liang, J. Min, L. Wang, and W. Shi, *J. Lumin.*, 2011, **131**, 1900.
53. H. Matsui and H. Tabata, *Appl. Phys. Lett.*, 2012, **101**, 231901.
54. H. Xue, N. Pan, M. Li, Y. Wu, X. Wang, and J. G. Hou, *Nanotechnology*, 2010, **21**, 215701.
55. K. E. Knutsen, a. Galeckas, Zubiaga, F. Tuomisto, G. C. Farlow, B. G. Svensson, and a. Y. Kuznetsov, *Phys. Rev. B*, 2012, **86**, 121203.
56. H. Chalabi and M. L. Brongersma, *Nat. Nanotechnol.*, 2013, **8**, 229.
57. H. M. et al Chen, *ACS Nano*, 2012, **6**, 7362.
58. J. M. Lin, H. Y. Lin, C. L. Cheng, and Y. F. Chen, *Nanotechnology*, 2006, **17**, 4391.
59. B. J. Niu, L. L. Wu, W. Tang, X. T. Zhang, and Q. G. Meng, *CrystEngComm*, 2011, **13**, 3678.
60. M. Liu, R. Chen, G. Adamo, K. F. MacDonald, E. J. Sie, T. C. Sum, N. I. Zheludev, H. Sun, and H. J. Fan, *Nanophotonics*, 2013, **2**, 153.
61. J. D. Hwang, Y. L. Lin, and C. Y. Kung, *Nanotechnology*, 2013, **24**, 115709.
62. M.W. Chen, C.Y. Chen, D.H. Lien, Y. Ding, and J.H. He, *Opt. Express*, 2010, **18**, 14836.
63. R. K. Joshi, Q. Hu, F. Alvi, N. Joshi, and A. Kumar, *J. Phys. Chem. C*, 2009, **113**, 16199.
64. A. Kushwaha and M. Aslam, *AIP Advances*, 2013, **3**, 042110.
65. D. B. Ingram and S. Linic, *J. Am. Chem. Soc.*, 2011, **133**, 5202.
66. C. Liu, X. Lu, Y. Tong, J. Z. Zhang, Y. Hsu, and Y. Li, *Nano Lett.*, 2013, **13**, 3817.
67. Z. Han, L. Wei, Z. Zhang, X. Zhang, H. Pan, and J. Chen, *Plasmonics*, 2013, **8**, 1193.
68. H. M. Chen, C. K. Chen, M. L. Tseng, P. C. Wu, C. M. Chang, L.C. Cheng, H. W. Huang, T. S. Chan, D.W. Huang, R.S. Liu, and D. P. Tsai, *Small*, 2013, **9**, 2926.
69. X. Yang, A. Wolcott, G. Wang, A. Sobo, R. C. Fitzmorris, F. Qian, J. Z. Zhang, and Y. Li, *Nano Lett.*, 2009, **9**, 2331.
70. S. Dhara and P. K. Giri, *J. Appl. Phys.*, 2011, **110**, 124317.